HHS Public Access

Author manuscript

Science. Author manuscript; available in PMC 2021 August 21.

Published in final edited form as:

Science. 2020 August 21; 369(6506): 942–949. doi:10.1126/science.aay2767.

BTN3A1 governs anti-tumor responses by coordinating alpha-beta and gamma-delta T cells*

Kyle K. Payne[1], **Jessica A. Mine**[1], **Subir Biswas**[1], **Ricardo A. Chaurio**[1], **Alfredo Perales-Puchalt**[2], **Carmen M. Anadon**[1], **Tara Lee Costich**[1], **Carly M. Harro**[1,3], **Jennifer Walrath**[2], **Qianqian Ming**[4], **Evgenii Tcyganov**[2], **Andrea L. Buras**[5], **Kristen E. Rigolizzo**[1], **Gunjan Mandal**[1], **Jason Lajoie**[6], **Michael Ophir**[6], **Julia Tchou**[7], **Douglas Marchion**[8], **Vincent C. Luca**[4], **Piotr Bobrowicz**[6], **Brooke McLaughlin**[6], **Ugur Eskiocak**[6], **Michael Schmidt**[6], **Juan R. Cubillos-Ruiz**[9], **Paulo C. Rodriguez**[1], **Dmitry I. Gabrilovich**[2], **Jose R. Conejo-Garcia**[1,5,#]

[1]Department of Immunology, H. Lee Moffitt Cancer Center & Research Institute, Tampa, FL 33612, USA.

[2]Immunology, Microenvironment & Metastasis Program, The Wistar Institute, Philadelphia, PA 19104, USA.

[3]Department of Cell Biology, Microbiology, and Molecular Biology and Cancer Biology PhD Program, University of South Florida, Tampa, FL 33620, USA.

[4]Department of Drug Discovery, H. Lee Moffitt Cancer Center & Research Institute, Tampa, FL 33612, USA.

[5]Department of Gynecologic Oncology, H. Lee Moffitt Cancer Center & Research Institute, Tampa, FL 33612, USA.

[6]Compass Therapeutics, Cambridge, MA 02142, USA.

[7]Division of Endocrine and Oncologic Surgery, Department of Surgery, University of Pennsylvania, Philadelphia, PA 19104-1693, USA.

[8]Department of Pathology, H. Lee Moffitt Cancer Center & Research Institute, Tampa, FL 33612, USA.

#**CORRESPONDENCE**: Jose R Conejo-Garcia, MD, PhD, H. Lee Moffitt Cancer Center and Research Institute, 12902 Magnolia Drive, Tampa, FL 33612, jose.conejo-garcia@moffitt.org, Phone: (813) 745-8282, Fax: (813) 745-5580.

Competing interests: JRCG and DG are members of the External Advisory Board of Compass Therapeutics and receive consulting fees and stock options from the company. JRCG additionally receives consulting fees from Anixa Bioscience and Leidos. APP is the Vice President for Research & Development at Geneos Therapeutics. JL, MO, PB, BM, UE and MS were employees of Compass Therapeutics. JRCG, KKP, MMS, BTM and PB are inventors on patent application WO2020033923A1 submitted by Compass Therapeutics Llc, The Wistar Institute Of Anatomy And Biology and Moffitt Cancer Center, which covers a method for reducing CD277-mediated inhibition of alpha/beta T cells, as well as a method for inducing or enhancing CD277-mediated gamma/delta T cell stimulation.

Data and materials availability: The Crystal Structure of the human BTN3A1 ectodomain in complex with the CTX-2026 Fab was deposited in wwPDB (Accession code: PDB ID 6XLQ). The humanized BTN3A1 transgenic mouse, as well as CD45-ablated Jurkat cells transduced with CD45RA or CD45RO are available from JRCG under a material transfer agreement with Moffitt Cancer Center.

[9]Department of Obstetrics and Gynecology, Sandra and Edward Meyer Cancer Center, Weill Cornell Medicine, New York, NY 10065, USA.

Abstract

Gamma delta (γδ) T-cells infiltrate most human tumors, but current immunotherapies fail to exploit their *in situ* MHC-independent tumoricidal potential. Activation of γδ T-cells can be elicited by butyrophilin/butyrophilin-like molecules that are structurally similar to the immunosuppressive B7 family members. Yet how they regulate and coordinate αβ and γδ T-cell responses remains unknown. Here, we report that the BTN3A1 butyrophilin inhibits tumor-reactive αβ TCR activation by preventing segregation of N-glycosylated CD45 from the immune synapse. Notably, CD277 antibodies elicit coordinated restoration of αβ T-cell effector activity, and BTN2A1-dependent γδ lymphocyte cytotoxicity against BTN3A1^{+} cancer cells, abrogating malignant progression. Targeting BTN3A1 therefore orchestrates cooperative killing of established tumors by αβ and γδ T-cells, and could enable novel interventions for tumors resistant to existing immunotherapies.

One Sentence Summary:

BTN3A1 governs anti-tumor T-cells

MAIN TEXT

The advent of immune checkpoint inhibitors has revolutionized the management of certain cancers (1-3). However, most solid tumors remain poorly responsive to existing immunotherapies, and the dramatic success of PD-1-targeting antibodies for melanoma and lung cancer are not frequently observed in other tumor types. While most immunotherapeutic approaches focus on boosting αβ T-cell responses, other leukocyte subsets with anti-tumor potential infiltrate tumor beds. In ovarian cancer, a disease resistant to single checkpoint blockade, ~6% of hematopoietic cells in solid tumors (>20% of CD3^{+} T-cells) represent γδ T-cells (4), which include Vγ9Vδ2 lymphocytes; the most abundant γδ T-cells in peripheral blood (5-8). Although γδ T-cells spontaneously exhibit regulatory activity at tumor beds through the production of galectin-1 (4), there is a strong rationale for rescuing their anti-tumor activity in coordination with effector αβ T-cells, to expand the range of immunotherapy-sensitive tumors.

The extracellular domains of butyrophilin (BTN) and butyrophilin-like (BTNL) molecules are structurally related to the B7 family of costimulatory ligands, which includes PD-L1, B7-H3 and B7-H4 (9). Polymorphisms of several BTN and BTNL molecules are associated with inflammatory diseases (9-11), and it has been suggested that the BTN3A family of BTNs could modulate antigen-specific αβ T-cell responses, though the mechanism(s) remains unknown (12-15). More recently, BTN/BTNL molecules have been found to play critical roles in modulating γδ T-cell functions (16, 17), where concurrent BTN3A1:BTN2A1 interactions are essential for TCR-dependent activation of human Vγ9Vδ2^{+} T-cells (5, 6, 18-20). *In vivo* this is dependent on the binding of phosphorylated metabolites to the B30.2 intracellular domain (21, 22). However, these effects can be

mimicked by stabilizing the extracellular domain of BTN3A1 with CD277 (BTN3A1-3)-specific antibodies (23), possibly through multimerization of BTN3A1 and conformational changes from its spontaneous V-shaped conformation (19, 22, 23).

We hypothesized that the suppressive function of BTN3A1 against αβ T-cells occurs only in its spontaneous conformation without BTN2A1, and that antibodies targeting BTN3A1 would overcome the suppression of αβ T-cells and simultaneously induce γδ T-cell anti-tumor cytotoxicity. We report that anti-CD277 antibodies transform BTN3A1 from an immunosuppressive to an immunostimulatory molecule, thus dynamically eliciting coordinated αβ and γδ T-cell-driven antitumor immunity to abrogate the progression of established ovarian cancer.

RESULTS

BTN3A1 is overexpressed in aggressive human tumors to suppress αβ T-cell activity

To investigate the potential role of BTN3A1 in cancer, we first performed western blot using protein lysates from 42 stage III/IV human high-grade serous ovarian carcinomas (HGSOC). As shown in Fig.1A, BTN3A1 is heavily overexpressed in malignant tissues, compared to benign ovarian tumors and normal tissues. Slightly lower levels of a specific (~53 kDa) BTN3A1 band were found in 4 triple-negative breast cancers (TNBC) analyzed (Fig.1B), supporting that BTN3A1 expression is not restricted to ovarian malignancies. FACS analysis of freshly dissociated ovarian and breast carcinomas showed that CD277 expression was high among myeloid and tumor cells, with weaker expression found among lymphocytes (Fig.1C&D). Lower CD277 expression is retained on PBMCs from healthy donors, without differences between myeloid cells and lymphocytes (Suppl.Fig.1A).

Immunohistochemical analysis of 398 additional HGSOCs and 19 breast cancers of mixed histology confirmed that BTN3A1 is universally expressed at tumor beds, where it is commonly localized to the membrane and cytoplasm within epithelial cells (Fig.1E&Suppl. Fig.1B). Consistent with its immunosuppressive role, higher average BTN3A1 expression in 200 ovarian cancers with clinical annotations was significantly associated with reduced patient survival (Fig.1F). FACs analysis of an additional 13 HGSOCs confirmed Vγ9Vδ2 lymphocytes consist of up to 2.5% of total T-cells (Fig.1G), while γδ T-cell infiltration was associated with improved patients' outcome (Fig.1H&Fig.1I).

As predicted from its similarity to other B7 family members, BTN3A1 retrovirally expressed on the surface of MHC-I^{-}CD32^{+} K562 artificial antigen-presenting cells (BTN-K32 aAPCs) (24) abrogated OKT3-induced activation of both CD4^{+} and CD8^{+} αβ T-cells, sorted from the peripheral blood of multiple donors (Fig.2A). Similarly, HLA-A2-transduced BTN-K32 aAPCs pulsed with the NY-ESO-1 peptide SLLMWITQC (BTN-K32^{A2}) elicited similar blunting on specific TCR-transduced αβ T-cells(25) (Fig.2B&Suppl. Fig.1C). αβ T-cell suppression was independent of γδ T-cells (Suppl. Fig.1D) and was not due to phenotypic alterations in K562 cells, because similar inhibitory effects were observed using multiple clones of BTN3A1/mock-transduced aAPCs (Suppl. Fig.1E). Therefore, prognostically relevant BTN3A1 effectively suppress αβ T-cell responses.

Human anti-CD277 antibodies prevent BTN3A1-mediated inhibition of αβ T-cells while inducing γδ T-cell activation

To block the immunosuppressive activity of BTN3A1, a panel of 15 BTN3A1-reactive, full-length, monoclonal antibodies were obtained by screening a combinatorial human library expressed in a yeast presentation system (26). To avoid cross-linking, antibody-dependent T-cellular cytotoxicity and complement activation, these antibodies were generated on an aglycosylated human IgG1 backbone (27). Clone CTX-2026 was the most effective at restoring pMHC:TCR (Fig.2C&Suppl.Fig.1F) and OKT3 (Suppl.Figs.1G&1H) activation of $CD4^+$ and $CD8^+$ αβ T-cells, and advanced as the lead compound. As expected, CTX-2026 had no effect on T-cell proliferation using mock-transduced ($BTN3A1^-$) K32 or $K32^{A2}$ aAPCs (Suppl.Figs.1G&1I), Zoledronate treatment, which activates Vγ9Vδ2T-cells (19)] and CD277-specific Vγ9Vδ2-agonistic (clone#20.1 (23)) and antagonistic (clone#103.2 (28)) antibodies, restored BTN3A1-dependent αβ T-cell activation (Fig.2C&Suppl.Fig.1J). Accordingly, zoledronate and αCD277 antibodies also enhanced antigen-specific killing of NY-ESO-1-transduced, HLA-$A2^+BTN3A1^+$ OVCAR3 cells (NY-OVCAR3) (Fig.2D&Suppl.Fig.1K), and heightened cytotoxic elimination of $BTN3A1^+$ primary cancer cells from 3 HGSOCs by autologous tumor-infiltrating lymphocytes (Fig.2E&Suppl.Fig.1L)

To gain insights into the mechanism of CTX-2026 action, we determined the crystal structure of the CTX-2026-BTN3A1 complex (Suppl.Fig.2A). Notably, the F(ab) binds to the IgV domain of CD277 with a stoichiometry of 1:1. All three CDR loops of the heavy chain are involved in the paratope, with a minimal contribution from CDRL2 (Fig.2F). We superimposed this complex with the 20.1:CD277 complex (PDB 4F9L) to gain insight into the relative binding position of 20.1 and CTX-2026 (Suppl.Fig.2B). Importantly, epitope evaluation of CTX-2026 further revealed partial spatial and sequential overlap with clone 20.1 (Fig.2F, Suppl.Fig.2C, & Suppl.Files 1&2). Accordingly, *in vitro*, CTX-2026 (but not 103.2) re-directed the cytotoxic activity of Vγ9Vδ2 T-cells from multiple donors against $BTN3A1^+$ OVCAR3 cells (Fig.2G), or primary HGSOC cells (Fig.2H&Suppl.Fig3A), with the same efficacy as clone 20.1 or zoledronate.

Supporting recent reports (19, 20), CRISPR-mediated ablation of *BTN2A1* in BTN-K32 aAPCs (Fig.2I&Suppl.Fig.3B) abrogated antibody- and zoledronate-dependent IFNγ production by Vγ9Vδ2 T-cells (Fig. 2J). However, BTN2A1-ablated BTN-K32 aAPCs maintained their ability to suppress αβ T-cell activation (Fig.2K&Suppl.Fig3C), suggesting that the switch between the αβ immunosuppressive and Vγ9Vδ2 immunostimulatory activities of BTN3A1 is regulated by BTN2A1 signaling.

BTN3A1 suppresses αβ T-cells by preventing the segregation of CD45 from the immune synapse

To elucidate the mechanism by which BTN3A1 inhibits αβ T-cell activity, we confirmed that upon TCR activation, homodimeric BTN3A1-Fc (Suppl.Fig.3D) binding to the surface of activated primary T-cells -blunts the phosphorylation of TCR signaling molecules, as proximally as at activating residues in LCK^{Y394}, $Zap70^{Y319}$ and $CD3\zeta^{Y142}$ (Fig.3A). We excluded binding to potential immunosuppressive receptors by comparing the binding of recombinant GPR174, NRP1 and NRP2 Fc proteins to BTN-K32 versus mock-transduced

aAPCs (Suppl.Fig.3E). We next used BTN3A1-Fc proteins to co-immunoprecipitate (co-IP) the binding partner(s) of BTN3A1 on OKT3-activated primary αβ T-cells from multiple donors. In three independent experiments, liquid chromatography tandem mass spectrometry (LC-MS/MS) showed that BTN3A1 co-immunoprecipitated with a complex that consistently included only four T-cell proteins with an extracellular domain: CD3ε, CD3ζ, HLA-A and the phosphatase CD45, and also the intracellular TCR signaling protein LCK and the phosphatase PTPN6 (SHP-1) (Fig.3B&Suppl.File 3). CD45 similarly consistently co-immunoprecipitated with BTN3A1 from non-activated primary αβ T-cells and $CD45^+$ Jurkat cells (Suppl.Fig.3F&Suppl.File 4). In contrast, BTN3A1 did not reproducibly co-IP with other heavily glycosylated or abundant surface molecules, including CD44, CD5 or CD2. Accordingly, BTN3A1-Fc proteins bound to $CD45^+$ Jurkat cells, but not to CD45-ablated Jurkat cells (Suppl.Fig.3G), while ectopic expression of CD45RA or CD45RO (Suppl.Fig.3H) rescued BTN3A1-Fc binding (Fig.3C&Suppl.Fig.3I). Furthermore, *in situ* proximity ligation confirmed CD45:BTN3A1 interactions within ≤ 30-40nm on the T-cell surface (Fig.3D&Suppl.Fig.3J), while BTN3A1-Fc proteins (but not control PD-L1-Fc) pulled-down CD45 from activated αβ T-cells (Fig.3E). Whereas both CD45RA and CD45RO were found to directly bind to immobilized BTN3A1 proteins, binding to CD45RO was significantly stronger (Fig.3F). Notably, the extracellular IgV domain of BTN3A1 was sufficient to engage both isoforms (Fig.3G).

CD45:BTN3A1 interactions specifically drive αβ T-cell suppression, because CRISPR ablation of *PTPRC* in primary αβ T-cells (Suppl.Fig.3K) abrogated both the inhibitory effect of BTN3A1, and the rescuing effect of CTX-2026, while non-ablated $CD45^+$ T-cells in the same cultures were effectively suppressed and rescued (Fig. 3H&Suppl.Fig.3L).

Given these findings, we hypothesized that BTN3A1 might disrupt TCR triggering by preventing the segregation of CD45 from the immune synapse. To test this, a CD3ζ-GFP fusion protein was generated and was used to monitor the degree of CD3ζ:CD45 co-localization following OKT3-induced TCR triggering in the presence of BTN3A1-Fc versus control-Fc. As predicted, CD45 segregated from CD3ζ following TCR activation in the presence of control-Fc (Fig.3I). In contrast, the presence of BTN3A1 impeded the segregation of CD45 from CD3ζ in multiple independent experiments with different donors, further supporting that BTN3A1 abrogates αβ T-cell responses by effectively dismantling the immune synapse (Fig.3I&Suppl. Fig.4). We observed αβ T-cells activated in the presence of BTN3A1-Fc proteins (but not PD-L1-Fc) generated CD45-specific peptides approximately double the predicted size of monomeric CD45 under non-reducing conditions, (Suppl.Fig.5A&Suppl.File 5), indicative of inhibitory CD45 dimerization (29). However, while $CD45^-$ Jurkat cells were not sensitive to BTN3A1 suppression at TCR proximal residues as expected (Suppl.Fig.5B), CD45' Jurkat cells expressing CD45RO with an inactivating mutation in the cytoplasmic inhibitory wedge ($CD45RO^{E624R}$) remained sensitive to BTN3A1 inhibition at ^{Y394}LCK, which is consistent with localized CD45 within the immune synapse inhibiting pMHC:TCR ligation independent of its PTPase potential. (Fig.3J).

BTN3A1 binds to N-mannosylated residues in CD45

To elucidate how BTN3A1 binds to different isoforms of CD45, we focused on its heavily N-glycosylated residues (30). PNGase-treated (N-deglycosylated) primary T-cells (Fig.3K), $CD45^+$ Jurkat cells (Fig.3L&Suppl.Fig.5C), and $CD45^-$ Jurkat cells with ectopic expression of CD45RA and CD45RO (Suppl.Fig.5D&Suppl.Fig.5E) all showed significantly reduced binding to BTN3A1-Fc proteins, while surface level expression of CD45 remained intact (Suppl.Figs5C&5F). Similar results were obtained using the N-glycan inhibitor tunicamycin (Fig.3M&Suppl.Fig.5G), while conservative replacement of asparagine with aspartic acid in the extracellular domain of CD45RA also abrogated BTN3A1-Fc:Jurkat cells interactions (Fig.3N&Suppl.Fig.5H); all indicative of an N-glycosylation-dependent mechanism. Accordingly, N-deglycosylation by PNGase F or tunicamycin decreased CD45 co-immunoprecipitated with BTN3A1-Fc from activated αβ T-cells (Suppl.Fig.5I), whereas N-deglycosylation of either CD45RO or CD45RA by PNGase F abrogated their binding to immobilized BTN3A1 proteins (Fig.3O), while treatment of primary αβ T-cells with PNGase F abrogated the ability of BTN3A1 to blunt TCR proximal signaling in primary T-cells (Fig.3P). Corresponding results were observed using $CD45^-$ Jurkat cells transduced or not with CD45RO and CD45RA (Suppl.Fig.5B). However, PNGase F-mediated deglycosylation of BTN3A1-Fc did not abrogate binding to CD45RO (Suppl.Fig.5J), indicative of BTN3A1-specific N-glycan recognition.

Interestingly, CD45 mutants expressing only the membrane proximal fibronectin domains in CD45' Jurkat cells restored BTN3A1-Fc binding to an even greater extent than expression of CD45RA (Fig.3N), suggesting increased accessibility to proximal N-mannosylated oligosaccharides (30). Accordingly, mannan polysaccharides inhibited binding of BTN3A1-Fc proteins to αβ T-cells in a dose-dependent manner (Fig.3Q). Collectively, these data suggest that BTN3A1 recognizes N-mannosylated oligosaccharides within the membrane proximal domains of CD45, which anchors dimeric CD45 near the TCR and blunts effective TCR signaling, possibly by physically blocking pMHC:TCR ligation (31-34).

Anti-BTN3A1 antibodies elicit coordinated αβ and γδ T-cell responses to impede growth of established human ovarian tumors *in vivo*

To assess the potential of targeting BTN3A1 utilizing CTX-2026 to rescue human αβ T-cell responses against advanced tumors *in vivo*, we implemented the NY-OVCAR3 / αβ NY-ESO-1-specific TCR T-cell system (25) (Fig.4A, Suppl. Figs.1C&1K). Adoptive transfer of these (γδ T-cell-free) SLLMWITQC-reactive αβ T-cells only had modest effects in preventing the growth of established (75-250 mm^3) NY-OVCAR3 tumors compared to mock-transduced T-cells (Suppl. Fig.6A). In contrast, BTN3A1 blockade with by CTX-2026 antibodies delayed malignant progression from 9 different donors (in 10 independent experiments) and was more effective than zoledronate and 20.1. (Fig.4B&Suppl.Figs.6B&6C). Superior therapeutic effects elicited by CTX-2026 were associated with significant increases in the accumulation of intratumoral antigen-reactive $CD8^+$ T-cells, compared to control IgG-treated mice (Fig.4C). Importantly, CTX-2026 was more effective than the anti-PD-1 antibody nivolumab when combined with tumor-reactive T-cells (Fig.4D and Suppl. Fig.6D), despite PD-L1 upregulation by NY-OVCAR3 tumor cells *in vivo* (Suppl. Fig.6E). Of note, tumors in all experiments were allowed to grow for at

least 15 days and were treated with a single T-cell injection, with significant growth delays for tumors as large as 300mm^3 at the time of adoptive transfer (Fig. 4A, Suppl. Figs.4A&4B).

Notably, the protective effects of CTX-2026 *in vivo* were not restricted to tumor-reactive αβ T-cells, because γδ T-cells from 8 different donors also elicited tumor growth reduction, albeit only in combination with CTX-2026 antibodies (Fig.4E and Suppl. Fig.6F). Accordingly, BTN3A1 targeting resulted in a greater accumulation of Vγ9 T-cells within tumor beds (Fig.4F). However, maximal anti-tumor responsiveness against established tumors was only achieved upon co-administration of γδ and tumor-specific αβ T-cells into NY-OVCAR3 tumor-bearing NSG mice in combination with CTX-2026 administration (Fig.4G&Suppl. Fig.6G) and was superior to zoledronate treatment (Suppl.Fig.6H). This provoked the formation of cystic cavities within the tumor (Fig.4H), indicative of partial tumor rejection. Thus, targeting BTN3A1 orchestrates coordinated responses between tumor-reactive αβ T-cells rescued from BTN3A1-mediated immunosuppression and cytotoxic Vγ9Vδ2 T-cells that are re-directed to kill BTN3A1$^+$ tumors.

Pre-existing anti-tumor immune responses in immunocompetent hosts are restored by anti-CD277 antibodies

To confirm the anti-tumor effectiveness of blocking BTN3A1 in myeloid cells in immunocompetent hosts, we engineered a knock-in mouse expressing human BTN3A1 under the control of the mouse *Itgax/Cd11c* promoter (BTN3A1^{KI}) (Fig.5A). As expected, CD11c$^+$ bone-marrow-derived dendritic cells (BMDCs) from BTN3A1^{KI} mice expressed human BTN3A1 on the cell surface (Fig.5B). Equally important, activation of murine T-cells in the presence of BTN3A1-Fc fusion proteins decreased IFN-γ release compared to controls (Suppl.Fig7A), while proliferation of OT-I T-cells in response to SIINFEKL-pulsed CD11c$^+$BTN3A1$^+$ BMDCs was significantly lower than in response to BTN3A1$^-$ BMDCs from littermates (Fig.5C&Suppl.Fig7B); thus, although mouse CD45 has a somewhat different pattern of glycosylation near the N-terminus, human BTN3A1 can also functionally suppress mouse αβ T-cells. Accordingly, treatment with anti-CD277 CTX-2026 also blocked human BTN3A1-mediated suppression of mouse αβ T-cells (Fig.5D&Suppl.Fig7C).

To test the role of BTN3A1 in an immunocompetent syngeneic ovarian cancer model, BTN3A1^{KI} mice were challenged i.p. with orthotopic ID%-Defb29/Vegf-a tumors, an aggressive model that responds to checkpoint inhibitors (35) and provokes the accumulation of tumor-promoting CD11c$^+$ myeloid cells (36). Predictably, compared to control littermates, BTN3A1^{KI} recipients accumulated BTN3A1$^+$ DCs in the ascites (Suppl.Fig.7D) and showed accelerated malignant progression (Suppl.Fig.7E). Targeting tumor-bearing BTN3AI^{KI} recipient mice with zoledronate extended their survival, but to a lesser extent than treatment with CTX-2026 and 20.1 antibodies (Fig.5E), with corresponding differences in intratumoral CD8$^+$ T-cell accumulation (Fig.5F). Consequently, the frequencies of peritoneal T-cells responding to cognate tumor antigen in IFN-γ ELISpot analyses were increased by all BTN3A1-targeting therapeutics, with the highest readout being for CTX-2026 (Fig.5G). Interestingly, murine γδ T-cells accumulated in the ascites of

BTN3A1^{KI} tumor-bearing mice in a CTX-2026-dependent manner (Fig.5H). As in our humanized model, targeting BTN3A1 was demonstrably more effective in delaying malignant progression than neutralizing the PD-L1/PD-1 checkpoint (Fig.5I). Thus, targeting BTN3A1 is able to overcome the highly immunosuppressive microenvironment of ovarian cancer, a disease that, thus far, has been resistant to existing checkpoint inhibitors.

DISCUSSION

We report that targeting BTN3A1 with novel human antibodies is sufficient to elicit coordinated αβ and γδ T-cell anti-tumor responses against established tumors and demonstrate that BTN3A1 targeting in validated orthotopic xenograft and syngeneic models of ovarian cancer is superior to PD-1 checkpoint therapy. Most human malignancies remain resistant to existing checkpoint inhibitors, which are aimed to rescue αβ T-cell responses. Yet, γδ T-cells also infiltrate multiple human cancers, where they primarily play regulatory roles (4, 37). Engaging the cooperation of these two T-cell subsets could therefore extend the range of cancer patients benefiting from immunotherapy. In addition, BTN3A1 -targeting was more effective than PD-1 neutralization in αβ T-cells in our PD-L1^{+} humanized systems, and it is possible that αCD277 antibodies may also block αβ T-cell inhibition by nearly identical BTN3A2 and BTN3A3. Because γδ T-cells also express PD-1, it will be interesting to determine whether coordinated action also takes place in patients that responder to checkpoint inhibitors. Nevertheless, unlike PD-L1, BTN3A1 does not require a specific receptor to mediate its immunosuppressive activity. Rather BTN3A1, independently of BTN2A1, inhibits αβ T-cells by binding to N-mannosylated residues in human CD45, preventing its segregation from the immune synapse and promoting its dimerization, thus abrogating effective TCR activation. At least in ovarian cancer, BTN3A overexpression in myeloid and tumor cells is associated with accelerated malignant progression, thus its possible that BTN3A1 targeting might be combined with other checkpoint inhibitors to enhance immunotherapeutic responses.

An interesting finding in our study is that both phosphometabolites and CTX-2026 antibodies transform BTN3A1 from an immunosuppressive to an immunostimulatory mediator. Recent work showed that phosphometabolite-driven co-signaling by BTN3A1 and BTN2A1 promotes Vγ9Vδ2 activation, while BTN2A1 is also required for the agonistic activity of antibody 20.1 (19). The structure of CTX-2026 bound to BTN3A1 is similar to that of mouse scFv 20.1:BTN3A complexes (23), in which both antibodies partially share an overlapping epitope. This supports the results of Adams and colleagues that agonistic antibodies modify the extracellular domains of BTN3A molecules, mimicking the effect of phosphoantigens (23). It is tempting to speculate that antibody/phosphoantigen-induced clustering separates BTN3A1 from MHC:antigen complexes, allowing robust engagement with specific αβ TCRs. However BTN2A1 is essential for antibody-driven switching of BTN3A1 from an immunosuppressive to immunostimulatory action, suggesting that CD277 clustering could release a BTN2A1 partner additionally required for Vγ9Vδ2 activation. Perhaps these mechanisms might be effectively elicited *in vivo* and *in situ* at tumor beds as a novel anti-cancer intervention.

Supplementary Material

Refer to Web version on PubMed Central for supplementary material.

ACKNOWLEDGEMENTS

Funding: Support for Shared Resources was provided by Cancer Center Support Grant (CCSG) CA076292 to H. Lee Moffitt Cancer Center. We are especially grateful to Chemical Biology, Analytic Microscopy, Advanced CLIA Tissue Imaging, Proteomics, and Flow Cytometry Shared Resources at Moffitt Cancer Center, as well as E. Larson of HarkerBio, for exceptional support. This study was supported by the National Institutes of Health (R01CA157664, R01CA124515, R01CA178687, R01CA211913 and U01CA232758 to JRCG; R01CA184185 to PCR; and R01NS114653 and R21CA248106 to JRCR); the U.S. Department of Defense Ovarian Cancer Research Program (W81XWH-16-1-0438 and W81XWH-20-1-0191 to JRCR), and Stand Up to Cancer (SU2C-AACR-IRG-03-16 and SU2C-AACR-PS24 to JRCR). KKP was supported by T32CA009140 and The American Cancer Society Postdoctoral Fellowship.

REFERENCES AND NOTES

1. Hellmann MD et al., Nivolumab plus Ipilimumab in Lung Cancer with a High Tumor Mutational Burden. N Engl J Med 378, 2093–2104 (2018). [PubMed: 29658845]
2. Motzer RJ et al., Nivolumab plus Ipilimumab versus Sunitinib in Advanced Renal-Cell Carcinoma. N Engl J Med 378, 1277–1290 (2018). [PubMed: 29562145]
3. Horn L et al., First-Line Atezolizumab plus Chemotherapy in Extensive-Stage Small-Cell Lung Cancer. N Engl J Med 379, 2220–2229 (2018). [PubMed: 30280641]
4. Rutkowski MR et al., Microbially driven TLR5-dependent signaling governs distal malignant progression through tumor-promoting inflammation. Cancer Cell 27, 27–40 (2015). [PubMed: 25533336]
5. Vavassori S et al., Butyrophilin 3A1 binds phosphorylated antigens and stimulates human gammadelta T cells. Nat Immunol 14, 908–916 (2013). [PubMed: 23872678]
6. Sandstrom A et al., The intracellular B30.2 domain of butyrophilin 3A1 binds phosphoantigens to mediate activation of human Vgamma9Vdelta2 T cells. Immunity 40, 490–500 (2014). [PubMed: 24703779]
7. Wang H et al., Butyrophilin 3A1 plays an essential role in prenyl pyrophosphate stimulation of human Vgamma2Vdelta2 T cells. J Immunol 191, 1029–1042 (2013). [PubMed: 23833237]
8. Meraviglia S et al., In vivo manipulation of Vgamma9Vdelta2 T cells with zoledronate and low-dose interleukin-2 for immunotherapy of advanced breast cancer patients. Clin Exp Immunol 161, 290–297 (2010). [PubMed: 20491785]
9. Rhodes DA, Reith W, Trowsdale J, Regulation of Immunity by Butyrophilins. Annu Rev Immunol 34, 151–172 (2016). [PubMed: 26772212]
10. Arnett HA et al., BTNL2, a butyrophilin/B7-like molecule, is a negative costimulatory molecule modulated in intestinal inflammation. J Immunol 178, 1523–1533 (2007). [PubMed: 17237401]
11. Abeler-Dorner L, Swamy M, Williams G, Hayday AC, Bas A, Butyrophilins: an emerging family of immune regulators. Trends Immunol 33, 34–41 (2012). [PubMed: 22030238]
12. Cubillos-Ruiz JR et al., CD277 is a Negative Co-stimulatory Molecule Universally Expressed by Ovarian Cancer Microenvironmental Cells. Oncotarget 1, 329–328 (2010). [PubMed: 21113407]
13. Yamazaki T et al., A butyrophilin family member critically inhibits T cell activation. J Immunol 185, 5907–5914 (2010). [PubMed: 20944003]
14. Sarter K et al., Btn2a2, a T cell immunomodulatory molecule coregulated with MHC class II genes. J Exp Med 213, 177–187 (2016). [PubMed: 26809444]
15. Messal N et al., Differential role for CD277 as a co-regulator of the immune signal in T and NK cells. Eur J Immunol 41, 3443–3454 (2011). [PubMed: 21918970]
16. Blazquez JL, Benyamine A, Pasero C, Olive D, New Insights Into the Regulation of gammadelta T Cells by BTN3A and Other BTN/BTNL in Tumor Immunity. Front Immunol 9, 1601 (2018). [PubMed: 30050536]

17. Di Marco Barros R et al., Epithelia Use Butyrophilin-like Molecules to Shape Organ-Specific gammadelta T Cell Compartments. Cell 167, 203–218 e217 (2016). [PubMed: 27641500]
18. Vantourout P et al., Heteromeric interactions regulate butyrophilin (BTN) and BTN-like molecules governing gammadelta T cell biology. Proc Natl Acad Sci U S A 115, 1039–1044 (2018). [PubMed: 29339503]
19. Rigau M et al., Butyrophilin 2A1 is essential for phosphoantigen reactivity by gammadelta T cells. Science 367, (2020).
20. Karunakaran MM et al., Butyrophilin-2A1 Directly Binds Germline-Encoded Regions of the Vgamma9Vdelta2 TCR and Is Essential for Phosphoantigen Sensing. Immunity 52, 487–498 e486 (2020). [PubMed: 32155411]
21. Gu S et al., Phosphoantigen-induced conformational change of butyrophilin 3A1 (BTN3A1) and its implication on Vgamma9Vdelta2 T cell activation. Proc Natl Acad Sci U S A 114, E7311–E7320 (2017). [PubMed: 28807997]
22. Yang Y et al., A Structural Change in Butyrophilin upon Phosphoantigen Binding Underlies Phosphoantigen-Mediated Vgamma9Vdelta2 T Cell Activation. Immunity 50, 1043–1053 e1045 (2019). [PubMed: 30902636]
23. Palakodeti A et al., The molecular basis for modulation of human Vgamma9Vdelta2 T cell responses by CD277/butyrophilin-3 (BTN3A)-specific antibodies. J Biol Chem 287, 32780–32790 (2012). [PubMed: 22846996]
24. Maus MV et al., Ex vivo expansion of polyclonal and antigen-specific cytotoxic T lymphocytes by artificial APCs expressing ligands for the T-cell receptor, CD28 and 4-1BB. Nat Biotechnol 20, 143–148 (2002). [PubMed: 11821859]
25. Robbins PF et al., Tumor regression in patients with metastatic synovial cell sarcoma and melanoma using genetically engineered lymphocytes reactive with NY-ESO-1. J Clin Oncol 29, 917–924 (2011). [PubMed: 21282551]
26. Jemal A et al., Cancer statistics, 2009. CA Cancer J Clin 59, 225–249 (2009). [PubMed: 19474385]
27. Ju MS, Jung ST, Aglycosylated full-length IgG antibodies: steps toward next-generation immunotherapeutics. Curr Opin Biotechnol 30, 128–139 (2014). [PubMed: 25035939]
28. Harly C et al., Key implication of CD277/butyrophilin-3 (BTN3A) in cellular stress sensing by a major human gammadelta T-cell subset. Blood 120, 2269–2279 (2012). [PubMed: 22767497]
29. Majeti R, Bilwes AM, Noel JP, Hunter T, Weiss A, Dimerization-induced inhibition of receptor protein tyrosine phosphatase function through an inhibitory wedge. Science 279, 88–91 (1998). [PubMed: 9417031]
30. Earl LA, Baum LG, CD45 glycosylation controls T-cell life and death. Immunol Cell Biol 86, 608–615 (2008). [PubMed: 18607388]
31. Chang VT et al., Initiation of T cell signaling by CD45 segregation at 'close contacts'. Nat Immunol 17, 574–582 (2016). [PubMed: 26998761]
32. Razvag Y, Neve-Oz Y, Sajman J, Reches M, Sherman E, Nanoscale kinetic segregation of TCR and CD45 in engaged microvilli facilitates early T cell activation. Nat Commun 9, 732 (2018). [PubMed: 29467364]
33. Irie-Sasaki J et al., CD45 is a JAK phosphatase and negatively regulates cytokine receptor signalling. Nature 409, 349–354 (2001). [PubMed: 11201744]
34. Hovis RR et al., Rescue of signaling by a chimeric protein containing the cytoplasmic domain of CD45. Science 260, 544–546 (1993). [PubMed: 8475387]
35. Stephen TL et al., SATB1 Expression Governs Epigenetic Repression of PD-1 in Tumor-Reactive T Cells. Immunity 46, 51–64 (2017). [PubMed: 28099864]
36. Tesone AJ et al., Satb1 Overexpression Drives Tumor-Promoting Activities in Cancer-Associated Dendritic Cells. Cell Rep 14, 1774–1786 (2016). [PubMed: 26876172]
37. Fleming C, Morrissey S, Cai Y, Yan J, gammadelta T Cells: Unexpected Regulators of Cancer Development and Progression. Trends Cancer 3, 561–570 (2017). [PubMed: 28780933]

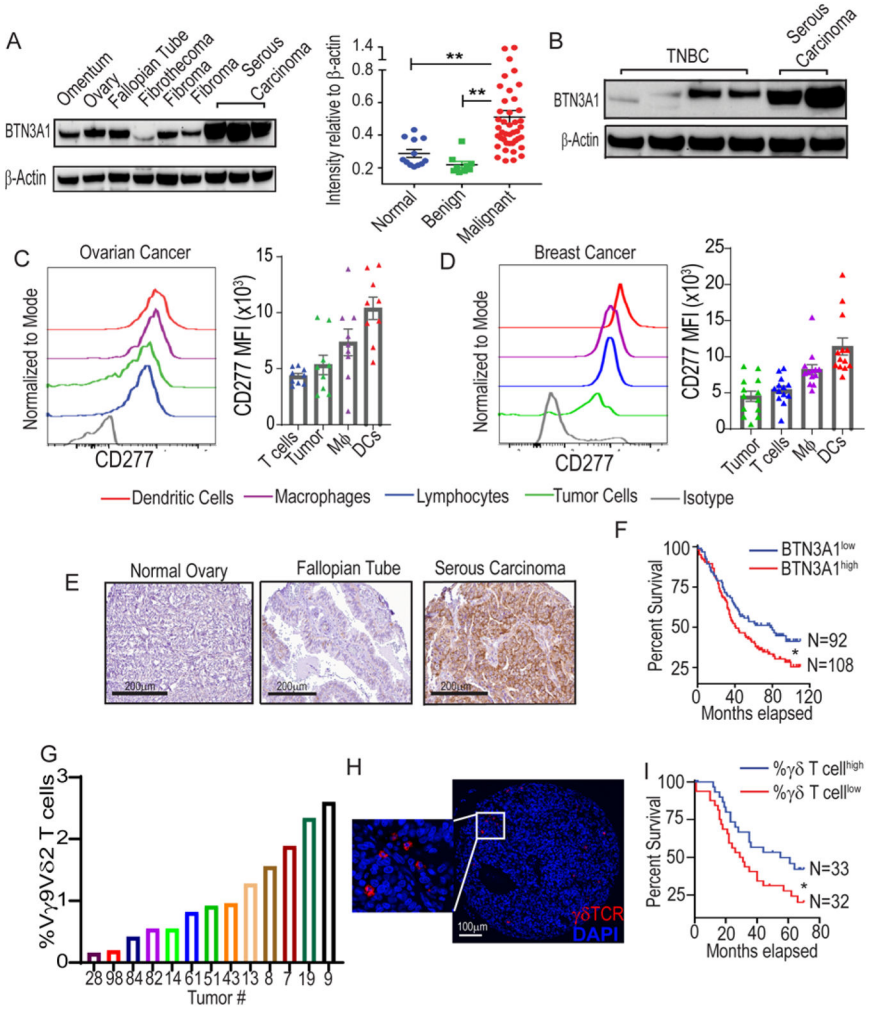

Figure 1. BTN3A1 is abundantly expressed in ovarian cancer and is associated with poor outcome.

(**A**) Relative expression of BTN3A1 in normal tissue (n=12), benign ovarian tumors (n=9), and ovarian serous carcinoma (N=42). Data represent mean ± SEM. (**B**) Expression of BTN3A1 in triple-negative breast cancer (n=4). (**C**) Expression of CD277 within dissociated human HGSOCs (n=9), data represent mean ± SEM, or (**D**) breast cancer of mixed histology (n=13) of dendritic cells ($CD45^+CD1c^+CD11c^+MHC\text{-}II^+Zbtb46^+$) and macrophages (Mϕ; $CD45^+CD1c^-CD11c^+MHC\text{-}II^+$), tumor cells ($CD45^-EpCAM^+$), and lymphocytes ($CD45^+CD1c^-CD11c^-MHC\text{-}II^-$) after normalization against the isotype control. Data represent mean ± SEM. (**E**) Representative BTN3A1 expression in indicated tissue samples as determined by immunohistochemistry. Scale bars represent 200 μm. (**F**) Survival outcome associated with the intensity of BTN3A1 expression within ovarian cancer specimens as assessed by IHC of TMAs corresponding to 200 independent ovarian cancer patients with clinical annotations. (**G**) Frequency of HGSOC-infiltrating Vγ9Vδ2 T-cells among total $CD3^+$ cells (n=13). (**H**) Multiplex Immunofluorescence detailing the presence of γδ T-cells (red) within HGSOCs. (**I**) Survival outcome associated with the frequency of γδ T-cells

within 65 HGSOCs with clinical annotations. Statistical analysis was performed as follows: One-way ANOVA (**a**); Log-rank (Mantel-Cox) test for survival (**f,i**). *p<0.05, **p≤0.01.

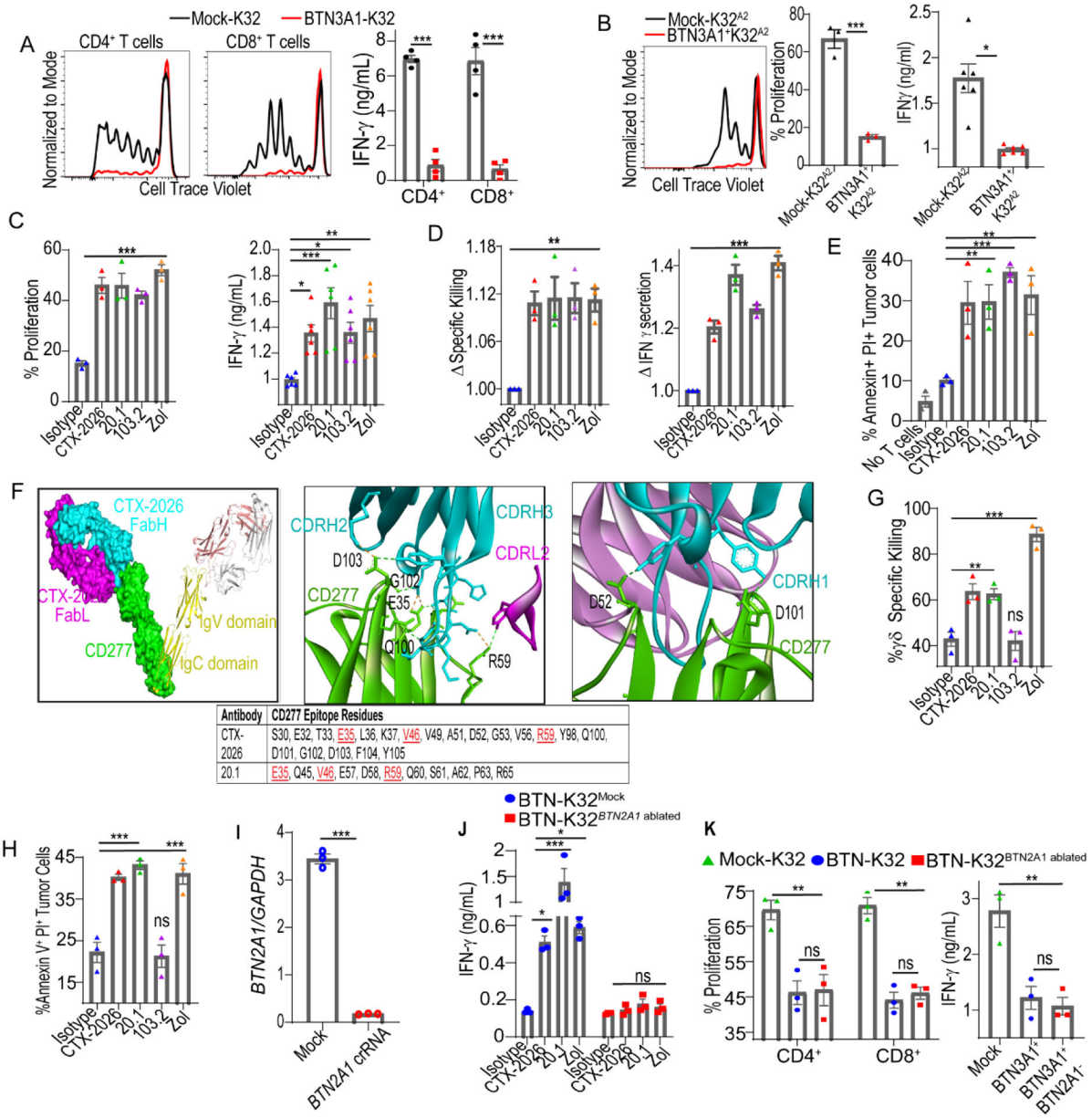

Figure 2. BTN3A1 specific antibodies relieve αβ T-cell inhibition and activate Vγ9Vδ2 T-cells.

(**A**) Proliferation and IFNγ release of CD4+ and CD8$^+$ T-cells cultured with OKT3 loaded (500ng/mL) BTN3A1-K32 or Mock-K32 cells at a 10:1 αβ T-cell:K32 ratio after 6 days. (**B**) Proliferation and IFNγ release of NY-ESO-1 TCR+ T-cells cultured with HLA-A2+ BTN3A1-K32 cells, or HLA-A2+ Mock-K32 cells, loaded with 1μM SLLMWITQV-peptide at a 10:1 T-cell:K32 ratio after 6 days. (**C**) Proliferation and IFNγ release after 6 days of NY-ESO-1 TCR+ T-cells cultured at a 10:1 T-cell:K32 ratio with HLA-A2$^+$ BTN3A1-K32 cells previously treated, or not, with zoledronate (1μM), loaded with 1μM SLLMWITQV-peptide and pre-incubated with 1μg/ml isotype control or anti-CD277 antibodies (CTX-2026, 20.1, or 103.2). (**D**) Specific killing of NY-ESO-1 TCR+ T-cells co-cultured with OVCAR3^{Luci} cells pretreated with 1μM zoledronate, or not, and pre-incubated with

1μg/mL isotype control or anti-CD277 antibodies (CTX-2026, 20.1, or 103.2) at a 10:1 αβ T-cell:Target cell ratio for 6 hrs. Data are represented as fold change relative to isotype control. (**E**) Cytotoxicity of immunopurified tumor-infiltrating $CD3^+$ αβ T cells from 3 HGSOC samples after co-culturing with matched tumor cells pretreated with 1μM zoledronate, or not, and pre-incubated with 1μg/mL isotype control or anti-CD277 antibodies (CTX-2026, 20.1, or 103.2) at a 5:1 αβ T-cell:Target cell ratio for 12 hrs. (**F**) Co-crystal structure of CTX-2026 interaction with CD277 homodimer in space-fill and ribbon diagram (left); interface highlighting hydrogen bonds between CD277 and CDRH2, CDRH3, and CDRL2 of CTX-2026 (middle) or CDRH1 of CTX-2026 (right); epitopes of CTX-2026 and 20.1, common residues are highlighted in red (bottom). (**G**) Similar to (D) except immunopurified γδ T cells were used at a 5:1 γδ T-cell:Target cell ratio for 24 hrs. (**H**) Similar to (E) except immunopurified γδ T cells were used at a 5:1 γδ T-cell:Target cell ratio for 24 hrs. (**I**) Relative quantity of *BTN2A1* mRNA in BTN-K32 cells electroporated with crRNA targeting *BTN2A1*, or not. (**J**) IFNγ release from immunopurified γδ T-cells co-cultured with BTN3A1-K32 cells, or BTN3A1-$K32^{BTN2A1\text{-}ablated}$ cells previously treated, or not, with zoledronate (1μM), and pre-incubated with 1μg/mL isotype control or anti-CD277 antibodies (CTX-2026, 20.1, or 103.2) at a 5:1 γδ T-cell:K32 ratio after 72 hrs. (**K**) Proliferation and IFNγ release of immunopurified αβ T-cells cultured with OKT3 loaded (500ng/mL) BTN3A1-K32 or BTN3A1-$K32^{BTN2A1\text{-}ablated}$ cells at a 10:1 αβ Tcell:K32 ratio after 6 days. For all histogram panels, data are representative of 3 independent experiments with similar results, and data represent mean ± SEM. Statistical analysis was performed as follows: Two-tailed Student's t-test (**b, i**) Two-way ANOVA (**a, j, k**); One-way ANOVA (**c, d, e, g, h, k**). ns: not significant, *$p<0.05$, **$p\leq0.01$, ***$p\leq0.001$.

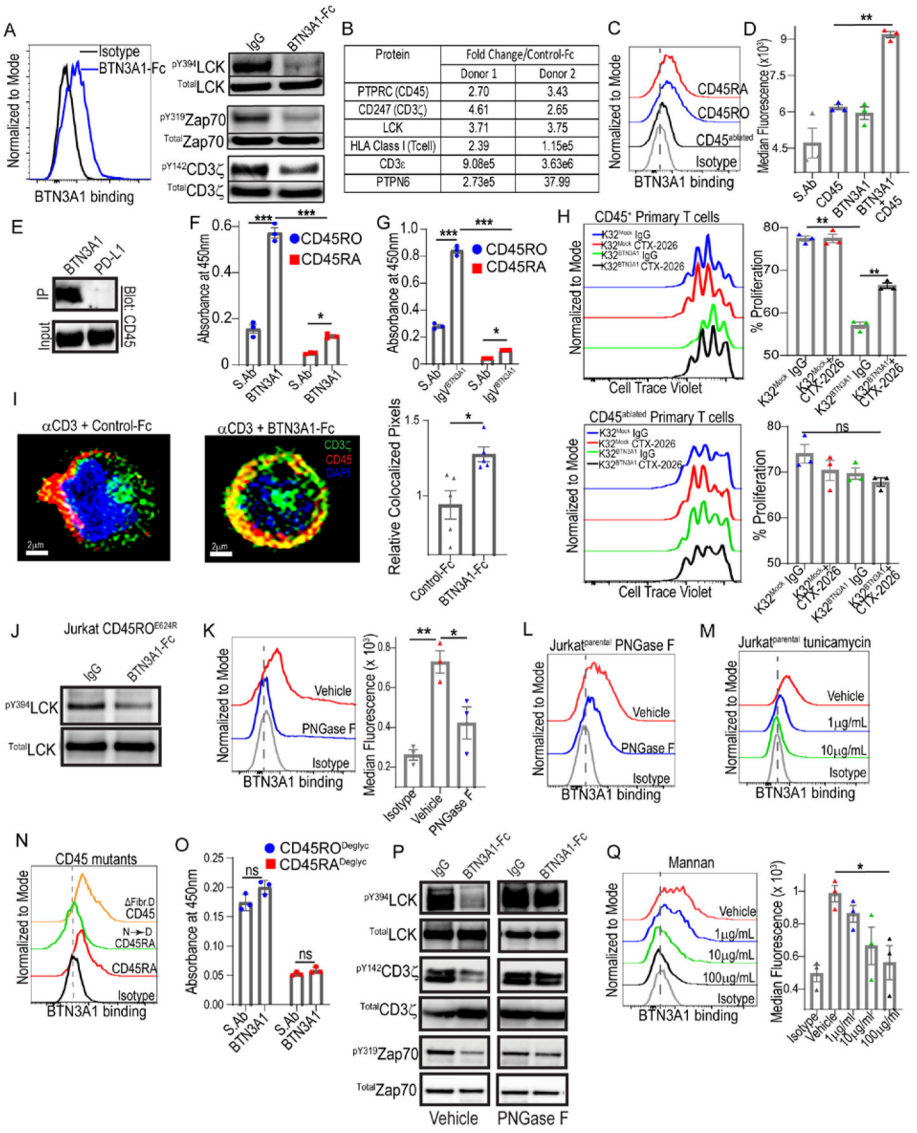

Figure 3. BTN3A1 interacts with the CD45 phosphatase, blunting proximal T-cell signaling events.

(**A**) Binding of BTN3A1-Fc to the surface of primary human T-cells (left); immunoblot of purified αβ T-cells after TCR crosslinking by plate-bound OKT3 in the presence of BTN3A1-Fc or control IgG-Fc proteins (all at 10μg/mL) for 1 min (right). (**B**) LC-MS/MS readout of BTN3A1-specific pulldowns after incubation with activated αβ T-cells. (**C**) Binding of BTN3A1-Fc to the surface of CD45- Jurkat cells or CD45- Jurkat cells with rescued expression of CD45RA or CD45RO. (**D**) *In situ* proximity ligation far red median fluorescence between BTN3A1 and CD45, single stained controls, or detection probes alone (S. Ab), using purified primary T-cells. (**E**) Immunoblot of CD45 after primary T-cells were coated with either BTN3A1-Fc or PD-L1-Fc (10μg/mL), lysed, and Fc protein immunopurification. (**F**) Absorbance at 450nm after immobilized BTN3A1 proteins (10μg/mL) were incubated with CD45RA or CD45RO proteins (20μg/mL) and CD45RA and CD45RO detection antibodies (20μg/mL), or after incubation of CD45RA or CD45RO

proteins (10μg/mL) and CD45RA and CD45RO detection antibodies (20μg/mL) without BTN3A1 immobilization (S.Ab). (**G**) Similar to (F), except only the IgV domain of BTN3A1 was immobilized. (**H**) Proliferation of CD45+ and CD45-ablated primary αβ T-cells cultured with BTN3A1-K32 cells or Mock-K32 cells in the presence or absence of 1μg/ml CTX-2026 or isotype control for 6 days. (**I**) Segregation of CD45 from CD3ζ in the presence of control-Fc or BTN3A1-Fc proteins (10 μg/mL) after TCR crosslinking in the presence of plate-bound OKT3 (10 μg/mL) for 3 minutes (left); cumulative quantification of CD3ζ and CD45 colocalization in the presence of BTN3A1-Fc or control-Fc proteins from 5 fields per condition with ~120 cells per field (right). Scale bars represent 2 μm. (**J**) Immunoblot of $CD45^{-}$ Jurkat cells expressing $CD45RO^{E624R}$ after TCR crosslinking by plate-bound OKT3 in the presence of BTN3A1-Fc or control IgG-Fc proteins (all at 10μg/mL) for 1 minute. (**K**) Binding (left), and median fluorescence (right), of BTN3A1-Fc proteins after primary T-cells were treated overnight with 100U/mL of PNGase F, or vehicle. (**L**) Binding of BTN3A1-Fc proteins to $CD45^{+}$ Jurkat cells after treatment overnight with 100U/mL PNGase F, or vehicle. (**M**) Binding of BTN3A1-Fc proteins to $CD45^{+}$ Jurkat cells after treatment with the indicated concentrations of Tunicamycin, or vehicle, for 72 hrs. (**N**) Binding of BTN3A1-Fc proteins to CD45- Jurkat cells or CD45- Jurkat cells expressing CD45RO, $CD45RO^{N\rightarrow D}$, or $CD45RO^{\Delta Fib.\ D}$. (**O**) Absorbance similar to (F), however N-linked glycans were removed from both CD45RA and CD45RO prior to the assay by overnight treatment with PNGase F. (**P**) Immunoblot similar to (A), however a portion of the primary T-cells were treated with PNGase F overnight (100U/mL) before the assay. (**Q**) Binding (left), and median fluorescence (right), of BTN3A1-Fc proteins after primary T-cells were pre-incubated with increasing concentrations of mannan polysaccharides, or vehicle. For all histogram panels, data are representative of 3 independent experiments with similar results, and represent mean ± SEM. Statistical analysis was performed as follows: Two-tailed Student's t-test (**i**) Two-way ANOVA (**f, g, o**); One-way ANOVA (**d, h, k, q**). ns: not significant, *$p<0.05$, **$p\leq0.01$, ***$p\leq0.001$.

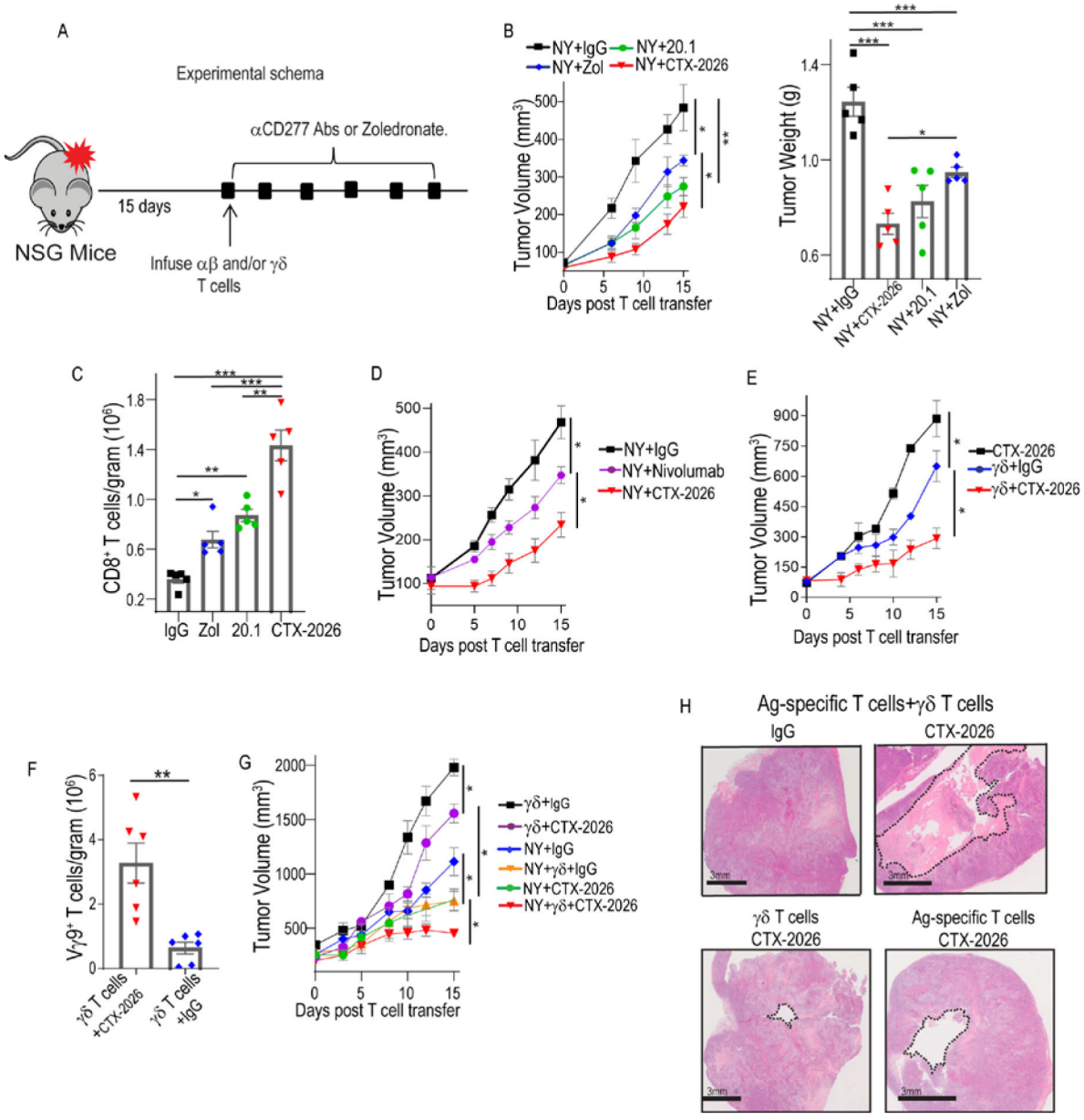

Figure 4. Targeting CD277 in vivo rescues Ag-specific αβ T-cell responses and leverages the cytotoxic potential of γδ T-cells.

(**A**) Experimental schema. (**B**) Progression of NY-OVCAR3 tumors in NSG mice treated with 1.5e6 NY-ESO-1-TCR transduced αβ T-cells and treated every third day with zoledronate (0.05mg/kg; i.p.), or CTX-2026, 20.1, or control IgG (5mg/kg; i.p.) (left); quantification of tumor weight from each group after 15 days (right). Data represent mean ± SEM with 5 mice/treatment group, representative of 3 independent experiments with similar results.. (**C**) Absolute number of GFP^+ $CD8^+$ αβ T-cells within NY-OVCAR3 tumors treated with zoledronate, CTX-2026, 20.1, or control IgG. (**D**) Progression of NY-OVCAR3 tumors in NSG mice treated with NY-ESO-1-TCR αβ T cells, and treated with Nivolumab©, CTX-2026, or control IgG every third day (5mg/kg; i.p.). Data represent mean ± SEM with 5 mice/treatment group, representative of 3 independent experiments with similar results..

(**E**) Progression of NY-OVCAR3 tumors in NSG mice treated with CTX-2026 or treated with 3e5 purified γδ T-cells and treated with CTX-2026 or control IgG, every third day. Data represent mean ± SEM with 3 mice/treatment group, representative of 3 independent experiments with similar results.. (**F**) Absolute number of γδ T-cells within NY-OVCAR3 tumors treated with CTX-2026, 20.1, or control IgG. (**G**) Progression of NY-OVCAR3 tumors in NSG mice treated with purified γδ T-cells and CTX-2026 or control IgG, αβ T-cells with CTX-2026 or control IgG, or the combination of Ag-specific αβ T-cells and autologous γδ T-cells (ratio of 6:1) with CTX-2026 or control IgG. Data represent mean ± SEM with 3 mice/treatment group, representative of 3 independent experiments with similar results. (**H**) Representative formation of cystic cavities in NY-OVCAR3 tumors treated with the combination of Ag-specific αβ T-cells, γδ T-cells and CTX-2026. Scale bars represent 3mm. Statistical analysis was performed as follows: Two-tailed Student's t-tests (**b** (left), **d, e, f, g**); One-way ANOVA (**b** (right), **c,).** *$p<0.05$, **$p\leq0.01$, ***$p\leq0.001$.

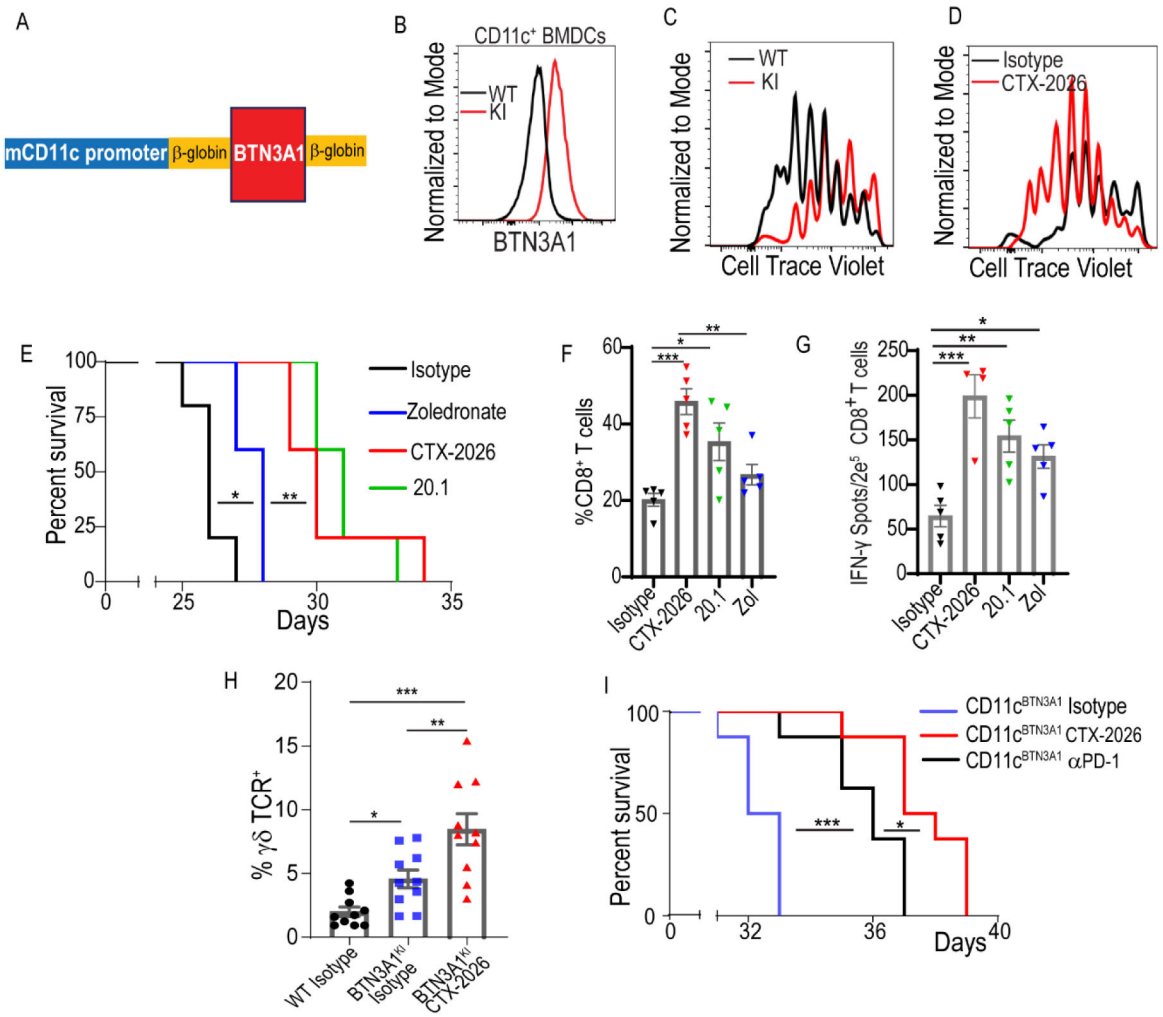

Figure 5. Targeting BTN3A1 rescues spontaneous anti-tumor immunity in BTN3A1^{tg} mice.

(**A**) Schematic of the CD11c-BTN3A1 construct. (**B**) BTN3A1 expression on BMDCs generated from wildtype C56/BL6 mice, or BTN3A1^{KI} mice. (**C**) Proliferation of OT-I T cells in the presence of WT-derived or BTN3A1^{KI}-derived BMDCs previously pulsed with 1 nM SIINFEKL peptide (left panel), and in the presence of CTX-2026 antibody (right panel) after 72hrs (**D**). (**E**) Survival of BTN3A1^{KI} mice bearing ID8-*Defb29-Vegf-a* peritoneal tumors treated every 5 days with zoledronate (n=5; 0.05mg/kg; i.p.), or CTX-2026 (n=5; 5mg/kg; i.p.), 20.1 (n=5; 5mg/kg; i.p.), or control IgG (n=5; 5mg/kg; i.p.), beginning 7 days after tumor challenge. (**F**) Frequency of CD8$^+$ T-cells among total CD3$^+$ T-cells in the ascites of BTN3A1^{KI} mice bearing ID8-*Defb29-Vegf-a* peritoneal tumors treated in (E). (**G**) Elispot readout comparing IFN-γ release from CD8$^+$ T-cells isolated from BTN3A1^{KI} mice bearing ID8-*Defb29-Vegf-a* peritoneal tumors at day 25, as treated in (E). (**H**) Frequency of γδ TCR$^+$ T-cells among total CD3$^+$ T-cells in the ascites of BTN3A1^{KI} mice, or WT C57/B16 mice, bearing ID8-*Defb29-Vegf-a* peritoneal, as treated in (E). Data represent mean ± SEM of 2 independent/5 replicate experiments. (**I**) Survival of BTN3A1^{KI} mice bearing ID8-*Defb29-Vegf-a* peritoneal tumors treated every 5 days with PD-1 neutralizing antibody (n=85mg/kg; i.p.), CTX-2026 (n=8; 5mg/kg; i.p.), or irrelevant IgG (n=8; 5mg/kg;

i.p.), beginning 7 days after tumor challenge. For figures F and G, data are representative of 3 independent experiments with similar results. Statistical analysis was performed as follows: Log-rank (Mantel-Cox) test for survival (**d, e**); Two-tailed Student's t-tests (**f**); One-way ANOVA (**g, h**). ns: not significant, *p<0.05, **p≤0.01, ***p≤0.001.